Available online at www.sciencedirect.com
ScienceDirect
Mechanical Systems and Signal Processing 22 (2008) 1441–1464
Mechanical Systems and Signal Processing
www.elsevier.com/locate/jnlabr/ymssp

# Damage characterization of polymer-based composite materials: Multivariable analysis and wavelet transform for clustering acoustic emission data

A. Marec[a], J.-H. Thomas[a,b], R. El Guerjouma[a,*]

[a]LAUM, CNRS, Université du Maine, Avenue Olivier Messiaen, 72085 Le Mans Cedex 9, France
[b]ENSIM, rue Aristote, 72085 Le Mans Cedex 9, France

Received 20 July 2007; received in revised form 26 November 2007; accepted 27 November 2007
Available online 23 December 2007

**Abstract**

In the present work, a procedure for the investigation of local damage in composite materials based on the analysis of the signals of acoustic emission (AE) is presented. One of the remaining problems is the analysis of the AE signals in order to identify the most critical damage mechanisms. In this work, unsupervised pattern recognition analyses (fuzzy C-means clustering) associated with a principal component analysis are the tools that are used for the classification of the monitored AE events. A cluster analysis of AE data is achieved and the resulting clusters are correlated to the damage mechanisms of the material under investigation. After being validated on model samples composed of unidirectional fiber-matrix composites, this method is applied to actual composites such as glass fiber/polyester cross-ply composites and sheet molding compound (SMC). Furthermore, AE signals generated by heterogeneous materials are not stationary. Thus, time-scale methods are used to determine new relevant descriptors to be introduced in the classification process in order to improve the characterization and the discrimination of the damage mechanisms. Continuous and discrete wavelet transforms are applied on typical damage mechanisms AE signals of glass fiber/polyester composites such as matrix cracking, fiber-matrix debonding. Time-scale descriptors are defined from these wavelet analyses. They provide a better discrimination of damage mechanisms than some time-based descriptors.


*Keywords:* Composite materials; Damage; Fracture; Acoustic emission; Pattern recognition; Wavelet analysis

## 1. Introduction

Glass fiber reinforced polymer (GFRP) composite materials are extensively used in industry. While their mechanical behavior is mostly well known, their damage and time-to-failure mechanisms still require a better understanding. One of the aims of this paper is to identify the most critical damage mechanisms occurring in these materials in order to estimate their remaining lifetime in a non-destructive way. Thus, acoustic emission

*Corresponding author. Tel.: +33 243833612; fax: +33 243833520.
*E-mail addresses:* anne.marec.etu@univ-lemans.fr (A. Marec), jean-hugh.thomas@univ-lemans.fr (J.-H. Thomas), rachid.elguerjouma@univ-lemans.fr (R. El Guerjouma).

0888-3270/$ - see front matter © 2008 Elsevier Ltd. All rights reserved.
doi:10.1016/j.ymssp.2007.11.029

(AE), which represents the generation of transient ultrasonic waves in a material under load, is a useful tool that can be used *in situ* for structural health monitoring [1,2]. Any generated AE signal contains useful information on the damage mechanism. One of the main issues of AE is to discriminate the different damage mechanisms from the detected AE signals. Most studies so far have used AE descriptors such as the amplitude and the energy of the signal to characterize the development of damage [3–9]. Each signal can be associated to a pattern composed of multiple relevant descriptors. Then the patterns can be divided into clusters representative of damage mechanisms according to their similarity by the use of multivariable data analyses based on pattern recognition algorithms [10]. As it is not possible to know exactly the origin of an emitted event and then to provide a training set of patterns belonging to several composite damage mechanisms, unsupervised pattern recognition is sometimes used with the problem of labelling the clusters [11–14]. Huguet et al. [15] use this approach for clustering AE events with a Kohonen's neural network [16] associated with the k-means algorithm [17]. They obtain interesting results on unidirectional fiber-matrix and cross-ply composites AE data during tensile tests. However, it is less effective for complex composite materials such as sheet molding compound (SMC), cross-ply composites under creep tensile tests for instance. In order to improve the classification process for complex composite materials, fuzzy C-means clustering [18,19] associated with a principal component analysis (PCA) [20,21] are proposed in this paper. The Fuzzy C-means Clustering Method (FCM) is an effective unsupervised algorithm for automatic clustering and separating AE patterns composed of multiple features extracted from the random AE waveforms. The PCA is first used to give an idea of the relevance of the descriptors. If the representation in the projection space shows several clusters with a minimum overlap between them, the features can lead to classify the damage mechanisms. The proposed method is applied to cross-ply and SMC composites under creep tensile tests. It permits to identify the damage mechanisms and to follow the time development of each damage mechanism till the final global fracture of the sample.

However, descriptor-based AE techniques often focus on time features which are not totally relevant for characterizing the AE waveforms especially for complex materials. First, other studies performed in the frequency domain have suggested that each damage mechanism is characterized by a different frequency peak obtained by Fourier analysis [22–24]. Ni et al. [25] investigate the characteristics of AE signals, such as the attenuation and the frequency dependency, during the fracture process of a single fiber composite. They show that the frequencies of AE signals are almost unchanged while the amplitudes attenuate greatly with the increment of the propagation distance between the AE source and the AE sensors. Since AE signals in composite materials are not stationary, time-frequency analysis has been first studied by the use of a short-time Fourier transform (STFT) as in [26] where frequency bands, evolving in time, characteristic of each damage mechanism are determined during tensile test on carbon/epoxy materials. Thus, waveform processing of AE signals based on time-scale or time-frequency analysis appears as a very promising signal processing technique to discriminate fracture mechanisms. Many previous works have shown that the continuous wavelet transform (CWT) brings an AE signal discrimination tool on different materials and under different kinds of load. Hamstad et al. [27] use a CWT to identify wideband analytical AE sources in aluminum plates. They show that the CWT representation is modified with the AE source type and the propagation distance between the AE sources and the AE sensors. Some studies have shown that the time-scale representation given by the CWT characterizes the failure mechanisms in composite materials. Ni et al. [25] investigate this point using a single fiber composite and Ferreira et al. [28] using GFRP composites under tensile and bending loading. Gallego et al. [29] use energy-position (percent of total scratch length)-scale wavelet diagrams in order to discriminate coating features related to adherence in scratch tests on galvanized steel. Some studies have used the time-scale representation of the CWT computed from typical AE signals in order to identify the different damage mechanisms in the composite materials. Suzuki et al. [30] obtain scalograms of AE signals from a longitudinal GFRP composite sample under tensile loading. The scalograms are classified into four types and correlated to the fracture dynamics. De Oliveira and Marques [31] use unsupervised pattern recognition algorithms based on artificial neural network to classify the AE data and then visualize time-scale diagrams of typical AE signal belonging to the obtained clusters. Thus, they identify six different AE waveforms acquired during tensile test of cross-ply glass fiber/polyester laminates. The discrete wavelet transform (DWT) is also used to discriminate AE signals. The DWT enables to decompose each signal into different continuous frequency bands which depend on the level of decomposition [32]. Thus, it is possible to determine with the

DWT the most energetic levels of decomposition and then identify the frequency bands representative of different damage mechanisms. Loutas et al. [33] use this approach in center-holed glass/polyester composites under quasi-static loading. They show from the energy of each level for all waveforms that the greatest percentage of energy is gathered in the range of 200–400 kHz. Some studies have shown that some descriptors extracted from the DWT can discriminate the failure mechanisms in composite materials. Qi et al. [34] apply the DWT on AE signals collected during static loading of unidirectional and cross-ply carbon-fiber-reinforced plastic (CFRP) composite materials. They define the energy rate and the percentage of total energy carried by the AE signal in each level of decomposition. Thus, they can identify the frequency bands and the percentage of the total energy representative of the different damage mechanisms associated with fracture of CFRP composites. Finally, Piotrkowski et al. [35] have defined a frequency-based descriptor from the DWT in order to identify different stages of coating adherence failure from scratch tests on stainless steel samples with Cr or Ti nitride coatings. This descriptor, corresponding to the frequency at which the spectral power density takes its maximum value for each signal, permits the identification of the different stages of failure.

In this paper, we investigate these wavelet transforms to provide relevant information from AE signals to discriminate the damage types. These two wavelet transforms are applied on typical matrix cracking and fiber-matrix debonding AE signals. We show that different time-scale distributions and different frequency bands characterize the two kinds of damage mechanisms. Due to the novelty of the use of both CWT and DWT in the field of AE data from composite materials, it is difficult to compare the results obtained with existing data. In addition, physical time-frequency parameters extracted from AE waveforms could enhance the monitoring and the detection of failure modes. Thus, we define new time-scale descriptors from the wavelet transforms. The results obtained are interesting since the new descriptors characterize very well each kind of damage mechanism. In the present paper, the studied materials then the mechanical and AE testing procedure are first introduced. The fuzzy C-means clustering associated with the PCA are both described in Section 3. The clustering results obtained from cross-ply and SMC composite materials are presented in Section 4. Then, the wavelet analysis applied on AE data is also reported in the last section in order to obtain relevant time-scale descriptors.

## 2. Experimental procedure

### 2.1. Description of the materials

The experimental work is carried out on GFRP composite materials. Cross-ply composites and SMC are studied as in [8,36]. Rectangular plates of cross-ply composites are obtained by a hand lay up technique in the lab. This method consists in applying successively into a mold surface, a release agent, a layer of resin, a layer of unidirectional reinforcement and to impregnate the reinforcement by hand by means of a roller. Thus, cross-ply laminates noted $[\pm 62^\circ]_{12}$ are fabricated. The angles are measured with respect to the loading direction. The stacking sequence consists of 12 layers of unidirectional reinforcement. Composite materials are achieved at room temperature during approximately 24 h under pressure. The cross-ply composite specimens are in rectangular form and have dimensions $10 \times 100 \times 3\,\text{mm}^3$. The SMC composites consist of a combination of polyester resin, calcium carbonate filler, thermoplastic additive and random oriented short glass fibers. SMC composites are a more heterogeneous structure compared to the cross-ply composites. The SMC samples are in rectangular form and have dimensions $10 \times 100 \times 3\,\text{mm}^3$.

### 2.2. Mechanical testing procedure

Creep tensile tests are performed on fiber-matrix composite materials at room temperature using a Instron loading machine. A creep tensile test determines the deformation behavior under long-term static tensile stress. The specimens are subject to a remaining constant load while the strain is measured simultaneously (Fig. 1). Static three-point bending tests are performed using the same loading machine. The crosshead speed of the machine is fixed at 0.05 mm/min. The tests are repeated on three specimens of each configuration in order to investigate their reproducibility.

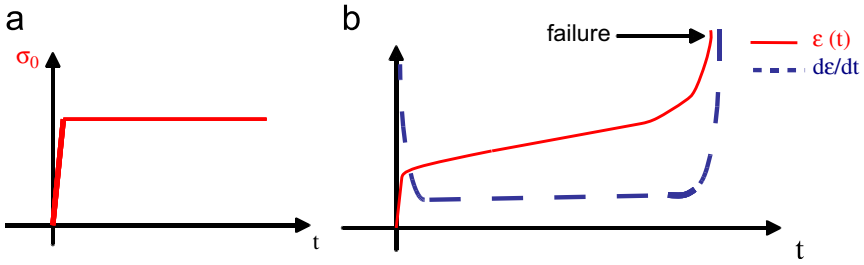


Fig. 1. Creep tensile test: (a) applied stress $\sigma_0$, (b) strain and strain rate responses: $\varepsilon(t)$ and $d\varepsilon/dt$.

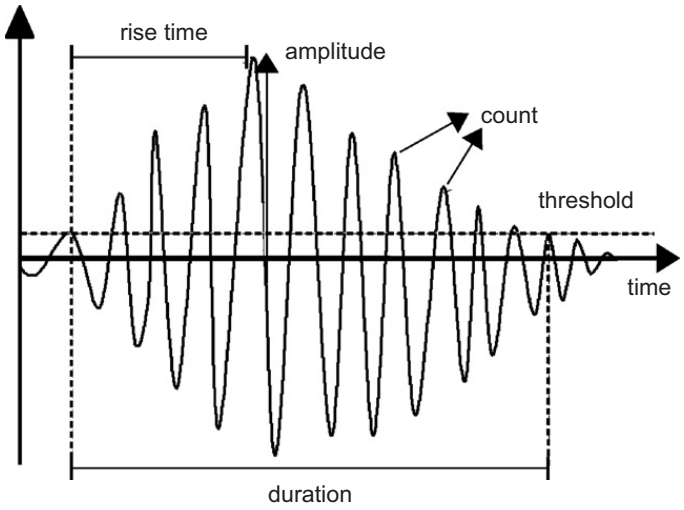


Fig. 2. Common waveform descriptors calculated by the acquisition system for each AE event.

### 2.3. Acoustic emission

An external load applied to the composite materials considered in this study results in inhomogeneous stress and strain fields which lead to a gradual damage development of the materials. Several damage mechanisms occur at a microscopic scale. GFRP composite materials have mainly four damage mechanisms: matrix cracking, fiber-matrix debonding, fiber failure and delamination [7,10,23,24]. However, some damage mechanisms are predominant depending on the composite material and the fiber orientation in comparison with the loading direction. All these damage mechanisms are coupled with an energy releasing called AE. The AE, which represents the generation of transient ultrasonic waves due to damage development within the material under load, is an efficient technique for structural health monitoring [1,2]. In this study, a two channel data acquisition system from Euro Physical Acoustics (EPA) corporation with a sampling rate of 5 MHz and a 40 dB pre-amplification is used to record AE data. AE measurements are achieved by using two piezoelectric sensors with a frequency range 100 kHz–1 MHz, coupled on the faces of the specimens with silicon grease. An amplitude threshold in the range from 32 to 46 dB is used to detect the arrival time and the end of an AE signal. The amplitude distribution covers the range 0–100 dB (0 dB corresponds to 1 μV for the transducer output). The acquisition system is calibrated before each test using a pencil lead break procedure [37], in order to estimate the velocity and the attenuation of the acoustic waves. The same average velocity has been measured in the cross-ply and SMC composites i.e. 2700 m/s. Several time-based descriptors are calculated by the acquisition system for each AE event (Fig. 2): the amplitude, the energy, the duration, the rise time, the number of times the amplitude of the event goes beyond the given amplitude threshold (called counts), etc. Only the amplitude of the signal is measured in real time by the data acquisition system. All the other descriptors are calculated from the waveforms and are very dependent on the amplitude threshold. These collected parameters are used as input descriptors in the proposed classification method. In addition, each waveform is stored in order to determine time-frequency or time-scale descriptors.

## 3. Multivariable data clustering

### 3.1. Fuzzy C-means

Unsupervised pattern recognition analyses provide a multidimensional data classification. The $d$ time-based parameters collected from $n$ AE waveforms are the components of the $n$ input pattern vectors $x_j$ $(j = 1, n)$. Each component provides information from the AE signals such as the amplitude of the signal, its energy, etc. Here the FCM [18,19] is used for the classification into $M$ classes representative of $M$ damage mechanisms. It uses fuzzy partitioning so that each pattern vector $x_j$ $(j = 1, n)$ can belong to each cluster $\omega_i$ $(i = 1, M)$ with different membership grades $u_i(x_j)$ between 0 and 1. FCM is an iterative algorithm. The aim of FCM is to find cluster centers $C_i$ that minimize the function $J$:

$$J(\mathbf{U}, \mathbf{V}) = \sum_{j=1}^{n} \sum_{i=1}^{M} [u_i(x_j)]^f d^2(x_j, C_i), \tag{1}$$

where $\mathbf{V}$ is the matrix of the cluster centers $C_i$:

$$\mathbf{V} = [C_1 | C_2 | \dots C_M], \tag{2}$$

and $\mathbf{U}$ is the membership matrix with $M$ lines and $n$ columns such as

$$\mathbf{U} = \begin{bmatrix} u_1(x_1) & u_1(x_2) & \dots & u_1(x_n) \\ u_2(x_1) & u_2(x_2) & \dots & u_2(x_n) \\ \vdots & \vdots & \vdots & \vdots \\ u_M(x_1) & u_M(x_2) & \dots & u_M(x_n) \end{bmatrix} \tag{3}$$

in which $u_i(x_j)$ represents the membership value of the $j$th pattern vector $x_j$ to the cluster $\omega_i$, under the condition

$$\sum_{i=1}^{M} u_i(x_j) = 1 \quad \forall j. \tag{4}$$

$f$ is a scalar which represents the fuzzy degree ($f = 2$). $d^2(x_j, C_i)$ is the distance between the pattern vector $x_j$ and the cluster center $C_i$ defined as

$$d^2(x_j, C_i) = (x_j - C_i)^t (x_j - C_i), \tag{5}$$

with $d^2(x_j, C_i)$ the square of the Euclidean distance, where $t$ represents the transpose of the matrix.

The input parameter of the algorithm is the number of clusters ($M$). In order to determine the appropriate number of clusters in the data set, two cluster validity criteria are used:

1. The partition coefficient (PC): This index measures the amount of "overlapping" between clusters. The "optimal" number of clusters is given by the maximum value of the index. It is defined as follows [19]:

$$PC(M) = \frac{1}{n} \sum_{i=1}^{M} \sum_{j=1}^{n} (u_i(x_j))^2. \tag{6}$$

2. The partition index (PI): This index aims at measuring the compactness of the clusters and the distances between the cluster centers. The cluster compactness is described by the numerator of the index, the inter-cluster distances by the denominator. The lowest value of PI indicates the best partition. Indeed, compact clusters well separated in the representation space makes the classification more effective. The PI is

defined as [38]

$$PI(M) = \sum_{i=1}^{M} \frac{\sum_{j=1}^{n} (u_i(x_j))^f d^2(x_j, C_i)}{n \sum_{k=1}^{M} d^2(C_k, C_i)}. \tag{7}$$

The FCM algorithm runs with the following steps:

(a) The membership matrix $\mathbf{U}$ is randomly initialized with values (in [0,1]) that represent the membership values $u_i(x_j)$ of the $n$ patterns $x_j$ $(j = 1, n)$ to each cluster $\omega_i$ $(i = 1, M)$ according to Eq. (4).

(b) The new cluster centers $C_i$ are calculated from

$$C_i = \frac{\sum_{j=1}^{n} [u_i(x_j)]^f x_j}{\sum_{j=1}^{n} [u_i(x_j)]^f}. \tag{8}$$

(c) The membership matrix $\mathbf{U}$ is updated such as

$$u_i(x_j) = \left[ \sum_{k=1}^{M} \left[ \frac{d(x_j, C_i)}{d(x_j, C_k)} \right]^{2/(f-1)} \right]^{-1} \quad \text{for } i = 1, M \text{ and } j = 1, n. \tag{9}$$

Steps (b) and (c) are iterated until the improvement over the previous iteration is below a threshold $\varepsilon$, whereas $q$ are the iteration steps:

$$\|\mathbf{U}^q - \mathbf{U}^{q-1}\| < \varepsilon, \quad 0 < \varepsilon < 1. \tag{10}$$

By iteratively updating the cluster centers and the membership grades for each pattern, FCM iteratively moves the cluster centers to the "right" location within the data set. This procedure converges to a local minimum or a saddle point of $J$. Each cluster resulting from the classification corresponds to a different damage mechanism identified in the material but at this time, the damage mechanism is unknown. In order to associate each output cluster of the algorithm to the corresponding damage mechanism, the features of the patterns of each cluster are considered. As the amplitude of each AE signal is one of the most relevant time-based descriptors, the amplitude distribution of each obtained cluster is compared to results found in the bibliography which reports characteristics of damage types of composite materials [10,15,39]. Thus, each resulting cluster can be associated to the corresponding damage type. This method has been validated on model unidirectional fiber composite materials and provides an accurate classification even for actual complex materials such as cross-ply composites or SMC as reported in this paper.

### 3.2. Principal component analysis

The basic goal in PCA is to reduce the dimension of the data [20,21]. Indeed, a projection into a subspace of a very low dimension, for example two, is useful for visualizing the data. We consider the matrix population $\mathbf{X}$ composed of the $n$ patterns $x_j$:

$$\mathbf{X} = \begin{bmatrix} x_1^t \\ x_2^t \\ \vdots \\ x_n^t \end{bmatrix} = \begin{bmatrix} x_1^1 & x_1^2 & \dots & x_1^d \\ x_2^1 & x_2^2 & \dots & x_2^d \\ \vdots & \vdots & \vdots & \vdots \\ x_n^1 & x_n^2 & \dots & x_n^d \end{bmatrix}. \tag{11}$$

The data are first centered and reduced (the mean is null and the standard deviation is equal to unity for each column) then we calculate the covariance matrix:

$$\mathbf{C_X} = E[\mathbf{X}\mathbf{X}^t], \tag{12}$$

where $t$ represents the transpose of the matrix. The components of $\mathbf{C_X}$, denoted by $C_{kl}$ ($k = 1, d$ and $l = 1, d$), represent the covariances between the variables $x^k$ and $x^l$:

$$x^k = \begin{bmatrix} x_1^k \\ x_2^k \\ \vdots \\ x_n^k \end{bmatrix}, \quad x^l = \begin{bmatrix} x_1^l \\ x_2^l \\ \vdots \\ x_n^l \end{bmatrix}. \tag{13}$$

As the covariance matrix is a symmetric matrix, an orthogonal basis can be calculated by finding its eigenvalues and eigenvectors. The eigenvectors $e_k$ and the corresponding eigenvalues $\lambda_k$ are the solutions of the equation

$$\mathbf{C_X} e_k = \lambda_k e_k, \quad k = 1, 2, \ldots, d. \tag{14}$$

An ordered orthogonal basis can be created with the first eigenvectors having the direction of the largest variances of the data. Thus, directions in which the data set has the most significant amounts of energy can be found. Instead of using all the eigenvectors of the covariance matrix, we may represent the data in terms of only a few basis vectors of the orthogonal basis. If $\mathbf{A_K}$ ($d \times K$) is the matrix having the first $K$ eigenvectors, by transforming the data vector $\mathbf{X}$, we get

$$y = \mathbf{X}\mathbf{A_K}, \tag{15}$$

which represents the new coordinates of the $n$ patterns in the orthogonal coordinate system defined by the eigenvectors.

The PCA is applied on the matrix (with $n \times d$ dimensions) of the time-based parameters collected from AE waveforms. The PCA projection in a two-dimension space highlights the similarities between the patterns. If the data do not overlap, automatic discrimination between the damage classes can be considered. Thus, the choice of relevant features to compose the pattern can be validated. Results using this approach are given in the following section. PCA is also used here to visualize the clusters provided by the automatic classification performed with the FCM.

## 4. Results and discussion

### 4.1. Damage characterization: multivariable analysis of AE data

The composite materials described in this part are $[\pm 62^\circ]_{12}$ cross-ply and SMC composites as in [8,36,40]. These materials are experimented under creep tensile tests. The strain response of a creep tensile test on composite materials is generally divided into three parts: the primary creep which corresponds to a fast variation of the strain under the initial load, the secondary creep which corresponds to a quasi-constant strain rate and the tertiary creep in which the strain is fastly increased leading to the global failure of the material (Fig. 1). Different damage mechanisms have been identified on fiber-matrix composite materials from their AE signals [8,39,40]. According to those previous studies, the damage mechanisms that are considered according to the collected AE signals are: matrix cracking (characterized by signals called A signals), fiber-matrix debonding (B signals), delamination (D signals) for the cross-ply composite and matrix cracking (A signals), fiber-matrix debonding (B signals), fiber failure (C signals) for the SMC.

The multivariable analysis is applied in order to discriminate the damage mechanisms according to their AE patterns. In order to determine the number of clusters in each data set, the two cluster validity criteria described before: PC and PI, are used (see Figs. 3 and 4). From the evolution of the criteria, in particular the PI, with respect to the number of clusters, and from the fact that it is generally admitted that three damage mechanisms occur within the cross-ply composite or the SMC, the classification to make is considered as a three-class problem.

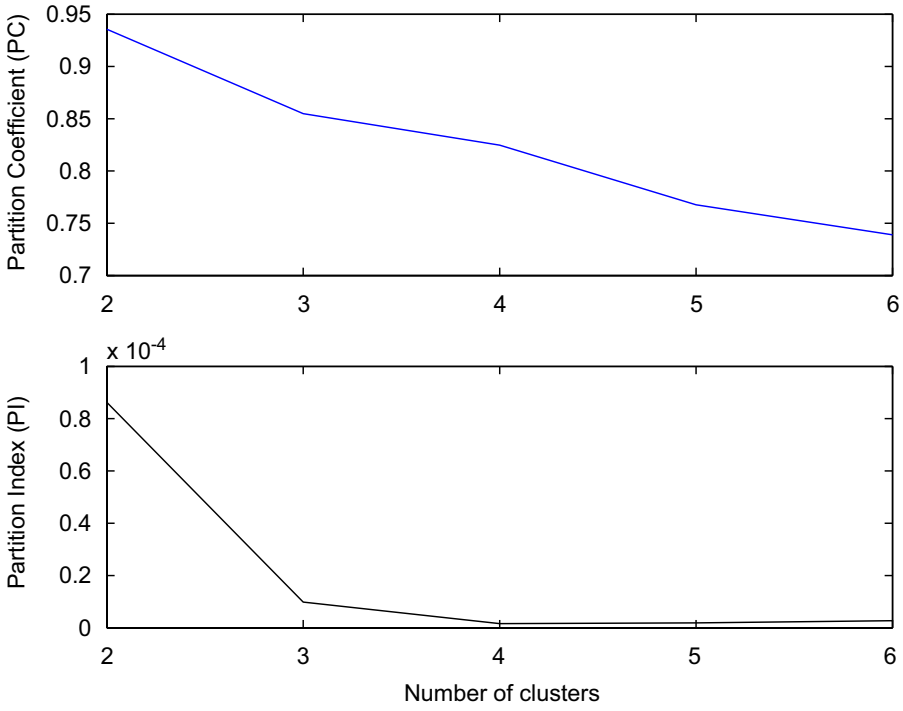


Fig. 3. Cluster validity criteria applied on $[\pm 62^{\circ}]_{12}$ cross-ply composite material.

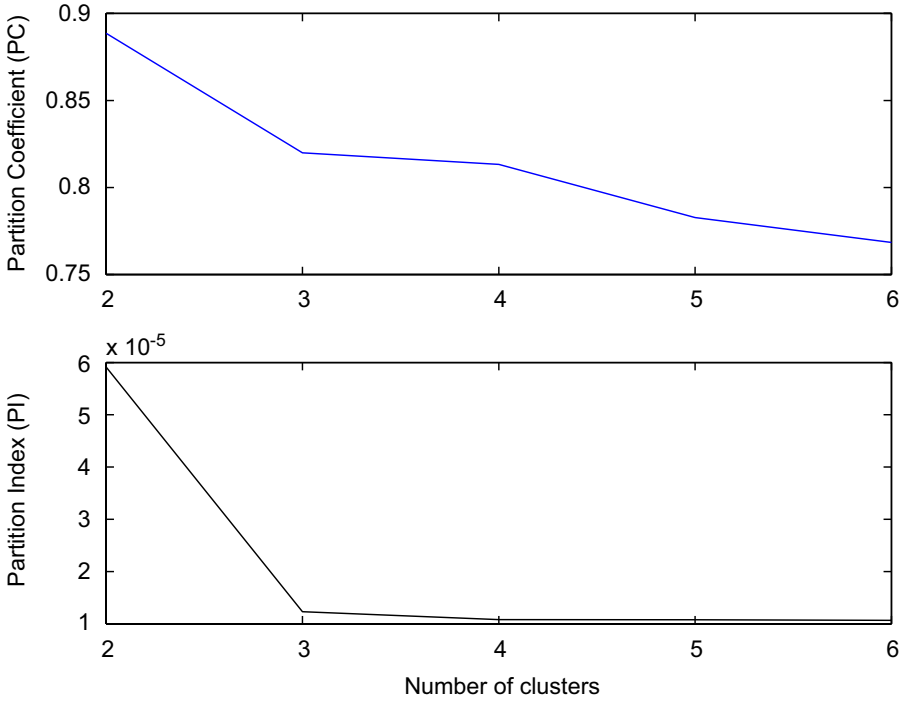


Fig. 4. Cluster validity criteria applied on SMC composite material.

Thus, the FCM is applied with three clusters. The five descriptors used are the energy, the amplitude, the rise time, the counts and the duration of the signals. A PCA is achieved in order to visualize the results in a two-dimension subspace (Figs. 5 and 6). The representation shows that most of the patterns are concentrated. Furthermore, the separation between the three classes provided by the FCM is consistent with the localization of the patterns according to the comparison made after clustering. Indeed, in order to know whether the three

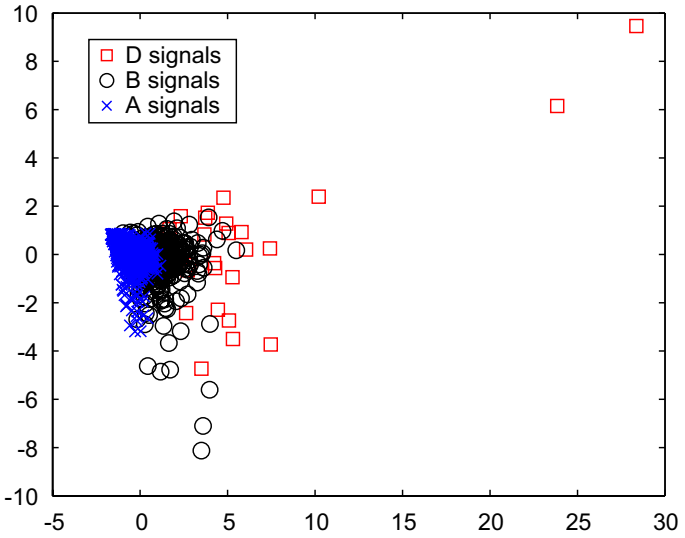


Fig. 5. PCA visualization of the fuzzy C-means clustering of creep tensile tests: $[\pm 62^{\circ}]_{12}$ cross-ply composite (82% information kept). A signal is representative of matrix cracking, B signal of fiber-matrix debonding and D signal of delamination.

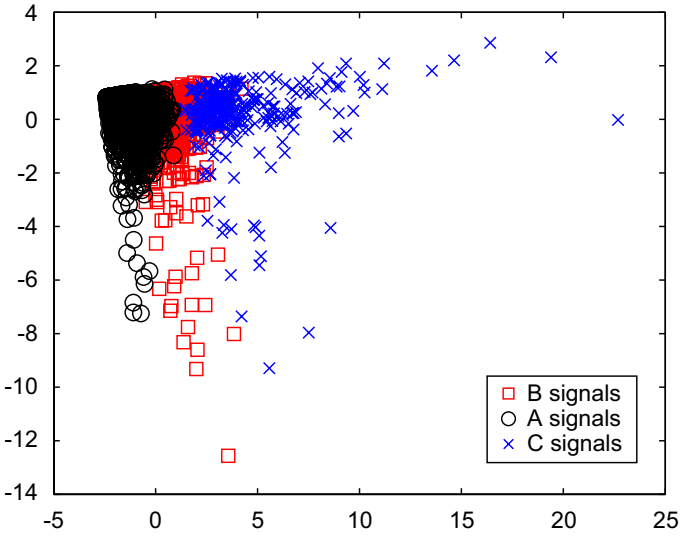


Fig. 6. PCA visualization of the fuzzy C-means clustering of creep tensile tests: SMC composite (89% information kept). A signal is representative of matrix cracking, B signal of fiber-matrix debonding and C signal of fiber failure.

identified clusters correspond to different damage mechanisms, we first compare the signals belonging to each resulting cluster with typical A, B, C and D signals representative of the different damage mechanisms in polymer-based composite materials. These typical signals are obtained from specific tests on model samples or on well-known composite materials found in the literature. In addition, the amplitude histograms of the patterns belonging to each cluster in comparison with results reported in the literature [10,15,39] lead to match the damage mechanisms with the clusters (Figs. 7 and 8).

The matrix cracking and the fiber-matrix debonding occur with delamination for the cross-ply composite material (1074 AE events). In the SMC composite (3427 AE events), we find the matrix cracking, the fiber-matrix debonding and the fiber failure. The identified A, B and D signals for the cross-ply composite and A, B and C for the SMC composite are presented in Figs. 9 and 10. These signals are similar to those reported in the literature [8,15,39].

Once the patterns are labelled in terms of damage mechanisms and since the arrival time of each AE event is stored, it is possible to show the time occurrence of the events provided by the different damage mechanisms

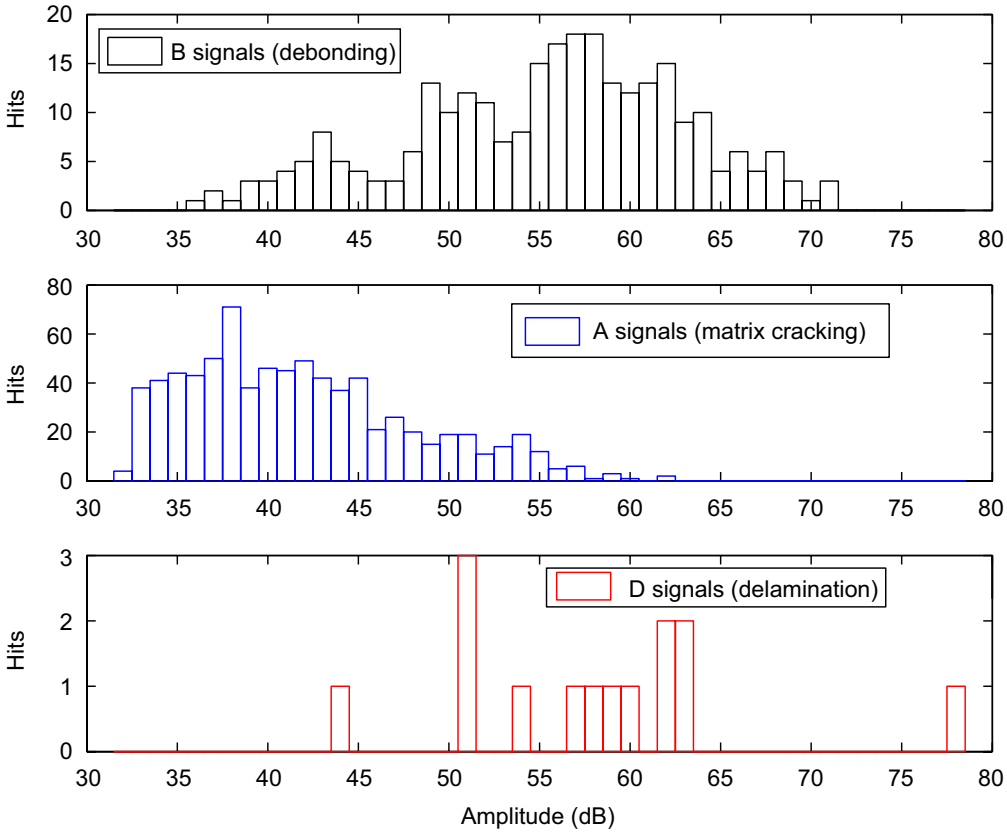


Fig. 7. Amplitude histograms of the patterns belonging to each cluster: $[\pm 62^{\circ}]_{12}$ cross-ply composite.

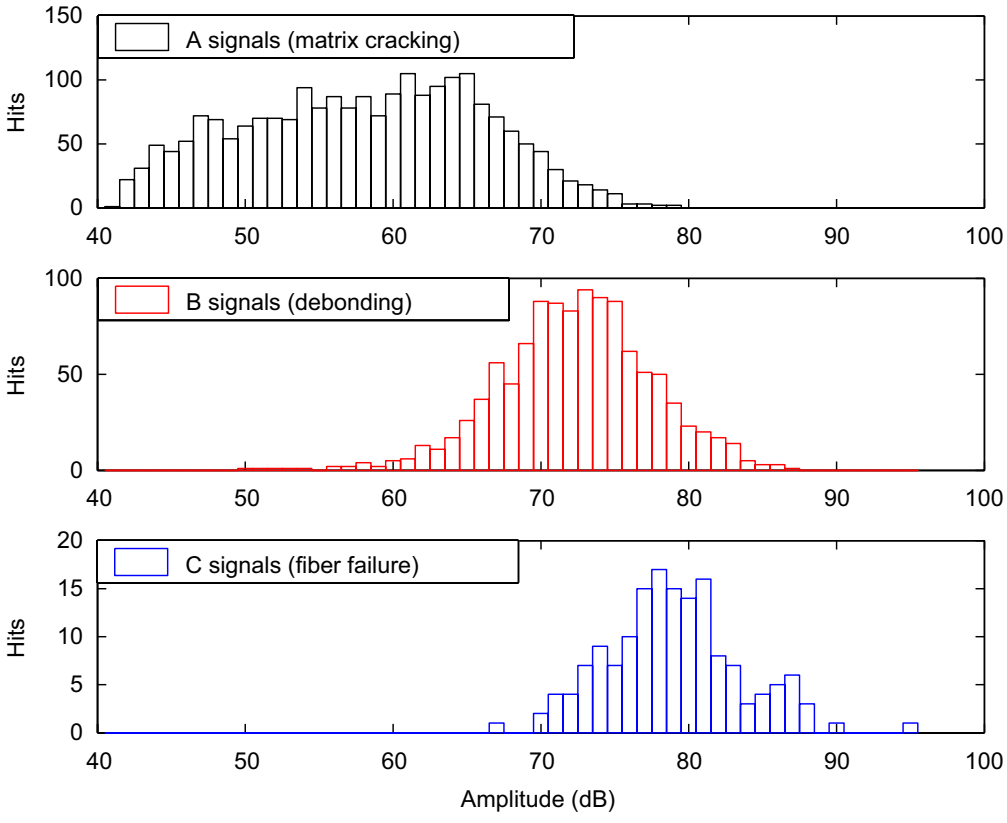


Fig. 8. Amplitude histograms of the patterns belonging to each cluster: SMC composite.

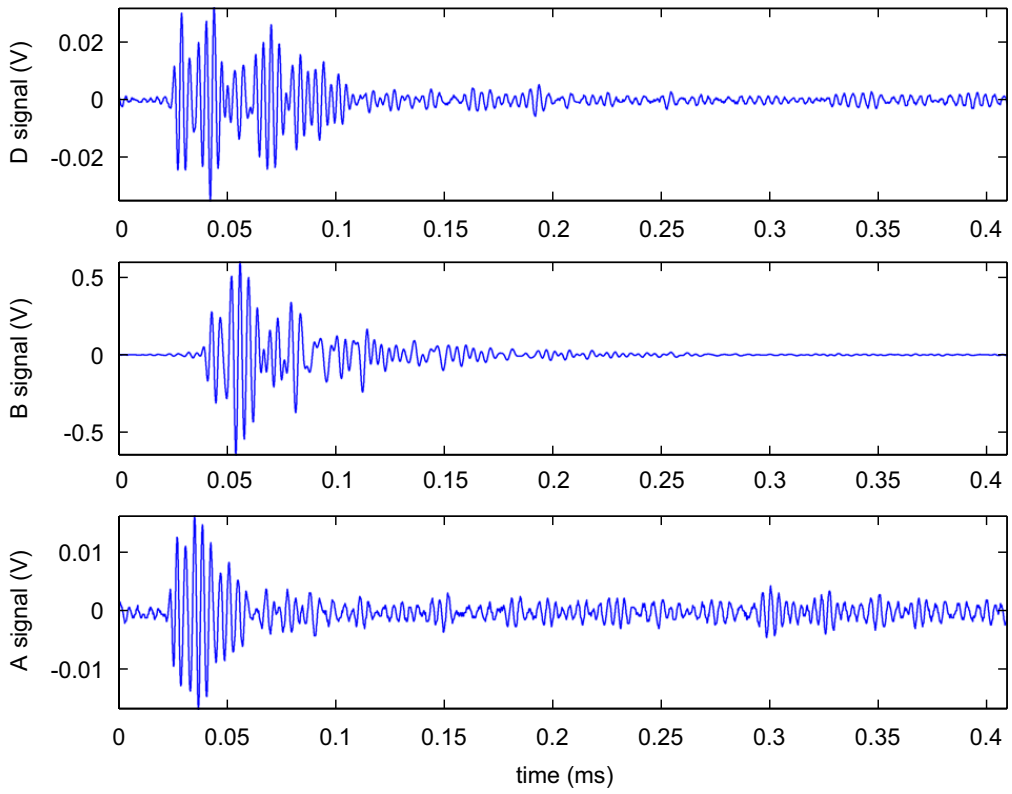


Fig. 9. AE signals of $[\pm 62^{\circ}]_{12}$ cross-ply composite: matrix cracking (A signal), fiber-matrix debonding (B signal) and delamination (D signal).

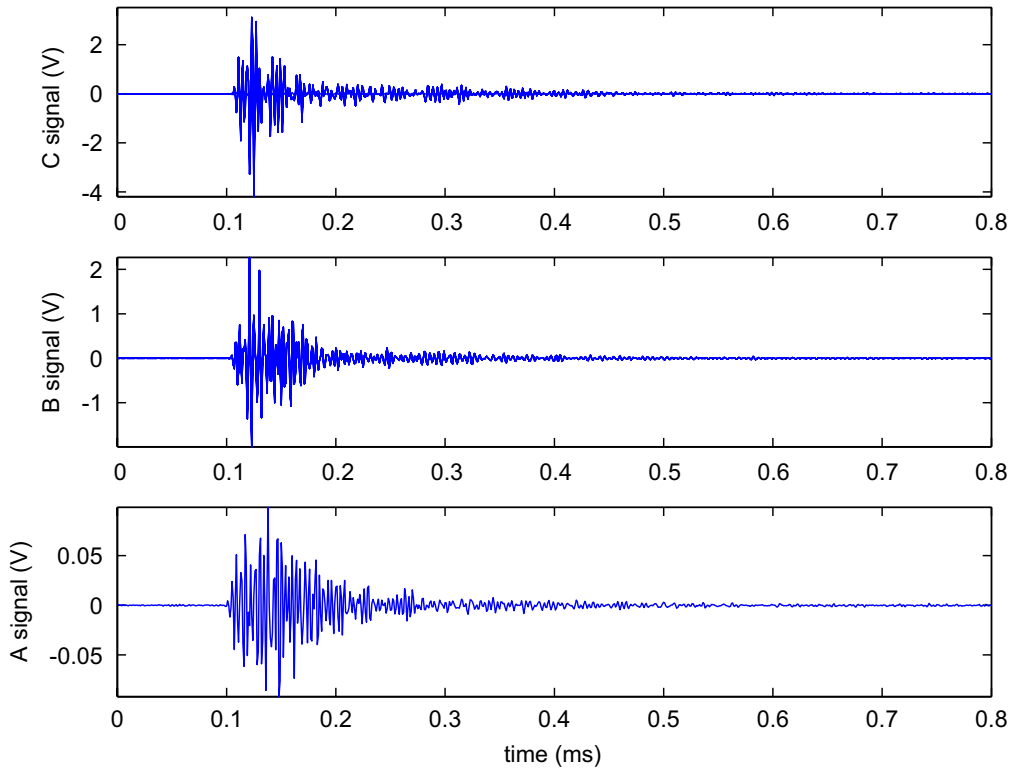


Fig. 10. AE signals of SMC composite: matrix cracking (A signal), fiber-matrix debonding (B signal) and fiber failure (C signal).

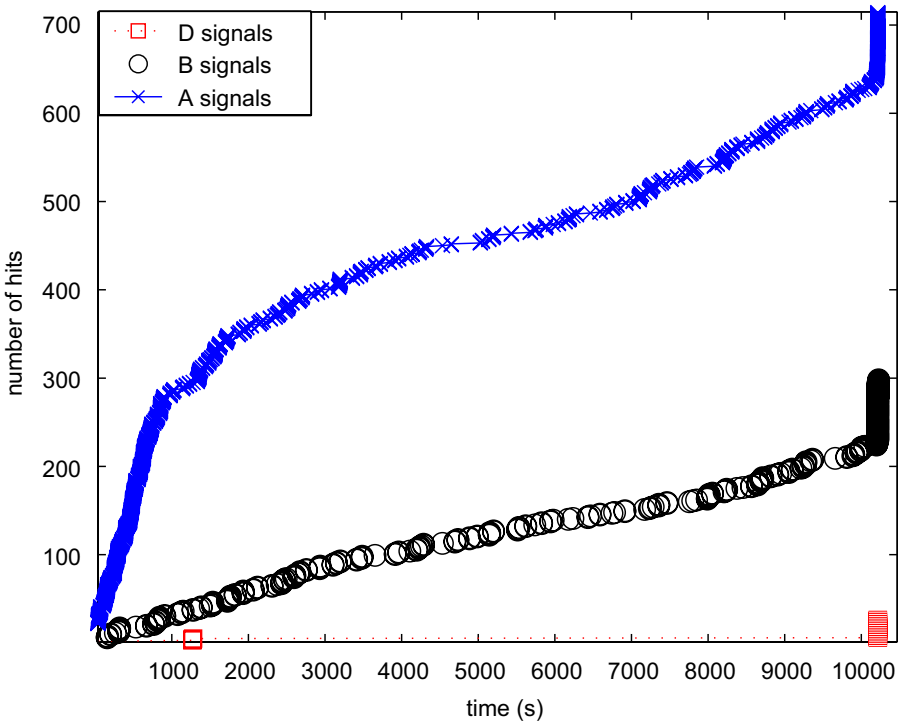


Fig. 11. Time dependency of the identified damage types during creep tensile tests: $[\pm 62^{\circ}]_{12}$ cross-ply composite. A signal is representative of matrix cracking, B signal of fiber-matrix debonding and D signal of delamination.

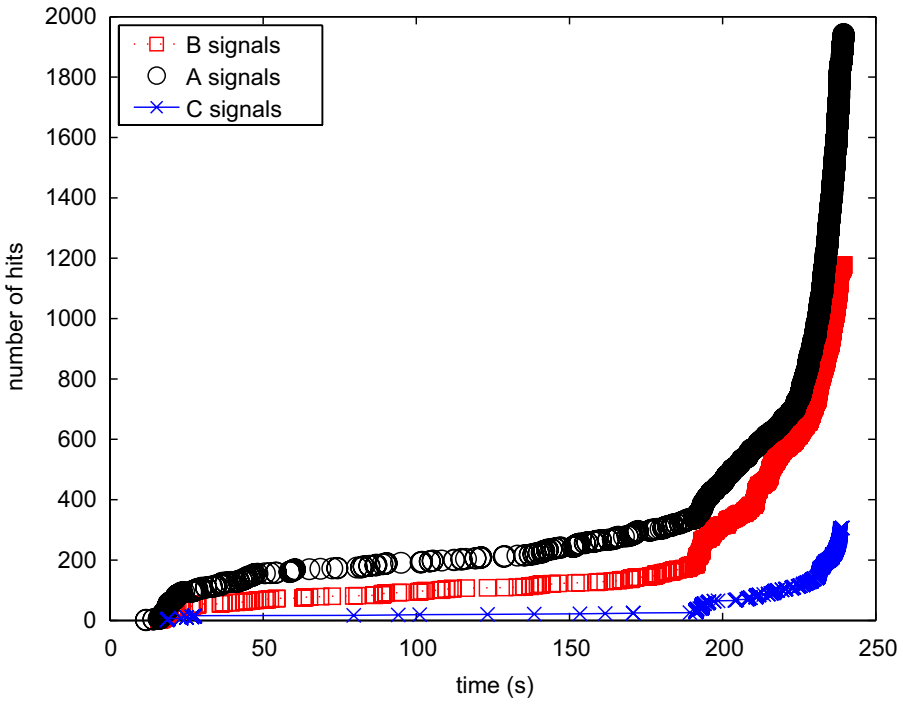


Fig. 12. Time dependency of the identified damage types during creep tensile tests: SMC composite. A signal is representative of matrix cracking, B signal of fiber-matrix debonding and C signal of fiber failure.

(Figs. 11 and 12). This visualization shows that before failure, the matrix cracking is the most dominant damage mechanism as it begins from the start of the tests and involves much more numerous AE events than the other mechanisms do (it involves 55% of AE events for the SMC and 65% for the cross-ply composite). The fiber-matrix debonding also appears from the start of the experiments and their number increases during

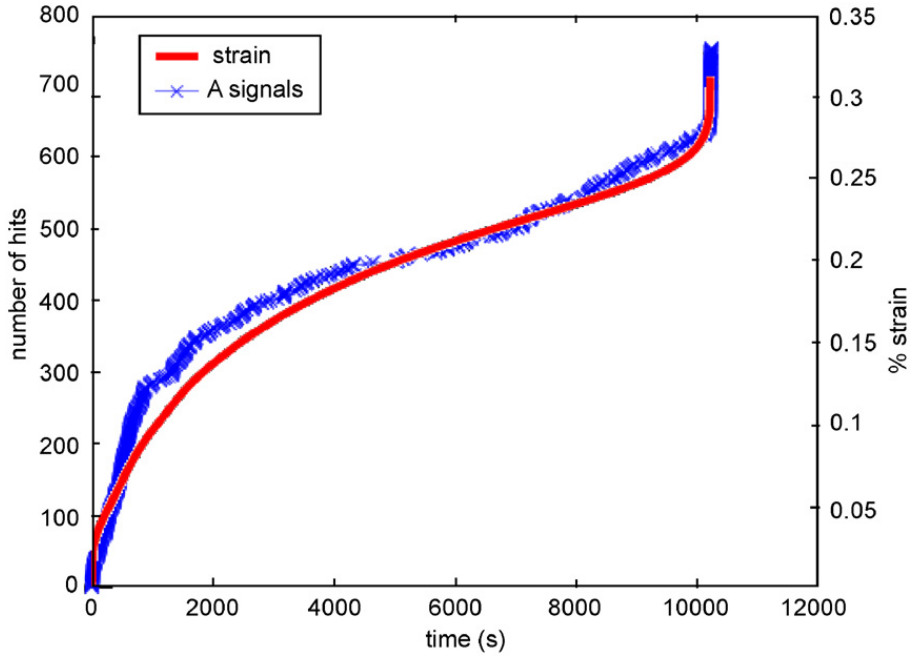


Fig. 13. Strain response and time dependency of matrix cracking (A signal) of the creep tensile test of $[\pm 62^{\circ}]_{12}$ cross-ply composite.

the tests (35% of AE events for the SMC and 30% for the cross-ply composite). For the cross-ply composite material, the delaminations (5% of AE events) mainly occur at the end of the tests and lead to the failure of the material. For the SMC composite material, the fiber fractures (10% of AE events) increase significantly at the end of the tests in the tertiary creep area and lead to the failure of the material. One can also note that the strain response of a creep tensile test fits the curve of the matrix cracking events in function of time (Fig. 13).

### 4.2. Time-scale analysis of AE data of composite materials: validation of the approach on a model material

As AE signals are not stationary and to enhance the relevance of the descriptors extracted from AE signals, a wavelet analysis is performed. To validate the approach, a model material in the form of unidirectional fiber-matrix composite is used. In order to generate two typical AE signals i.e. matrix microcracking (A signals) and fiber-matrix debonding (B signals), the sample is loaded with a loading direction at 45° according to the fiber direction. Thus, no fiber breaking is generated. The two obtained signals are presented in Fig. 14. B signals waveforms are quite different from the A signals waveforms, with shorter rise time, higher amplitudes and energies. The analysis is first validated on these two signals.

#### 4.2.1. Continuous wavelet transform

The CWT is a useful tool for the analysis of non-stationary signals [32]. The CWT of a signal $f(t)$ is defined as follows:

$$CW_f(a,b) = \frac{1}{\sqrt{a}} \int_{-\infty}^{\infty} f(t)\psi^*\left(\frac{t-b}{a}\right) \mathrm{d}t, \tag{16}$$

where $a$ is the scale parameter that stretches or compresses the mother wavelet $\psi(t)$, $*$ denotes the complex conjugation. The parameter $b$ is a time translation factor which simply shifts the wavelet, delaying or advancing the time at which it is activated. The Daubechies wavelets are used with 10 vanishing moments as the analyzing wavelets. They consist of orthogonal, compactly supported and not symmetrical wavelets with a good compromise of smooth function without sharp edges [41]. We chose these wavelets because their waveforms are similar to the studied transient AE signals and in comparison with Morlet wavelet, the lack of symmetry is more accurate. But as the Daubechies wavelet is not analytical, the implementation of the CWT with this wavelet is done using a time series for the mother wavelet obtained by successive convolutions

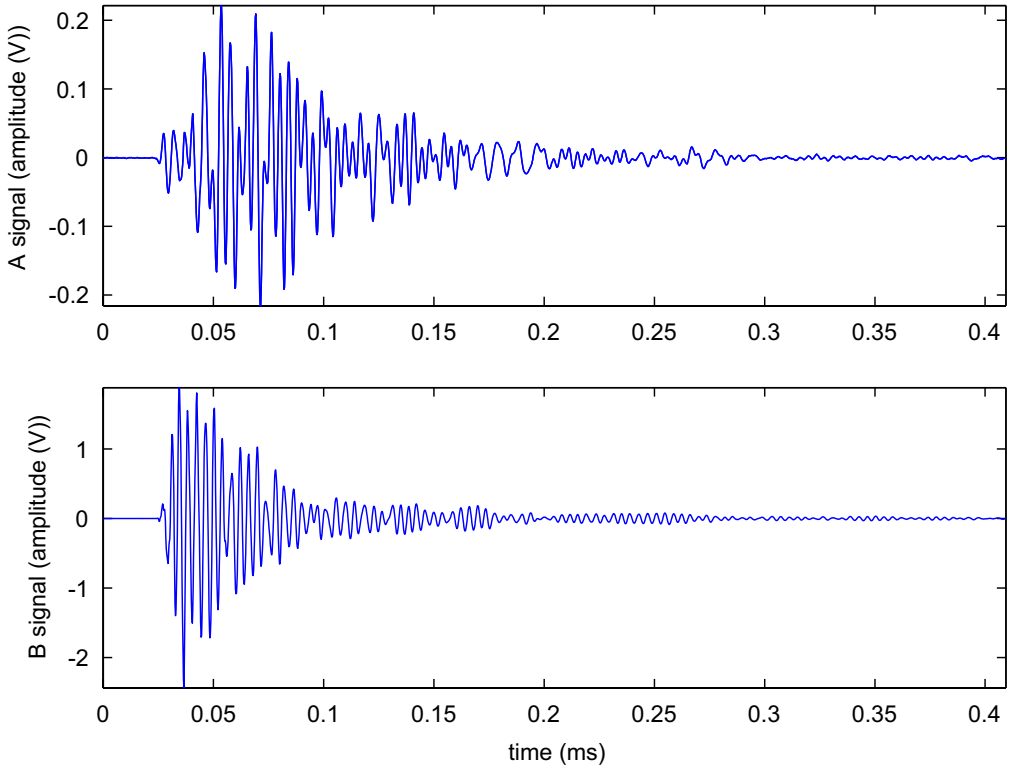


Fig. 14. AE typical signals: matrix cracking (A signal) and fiber-matrix debonding (B signal).

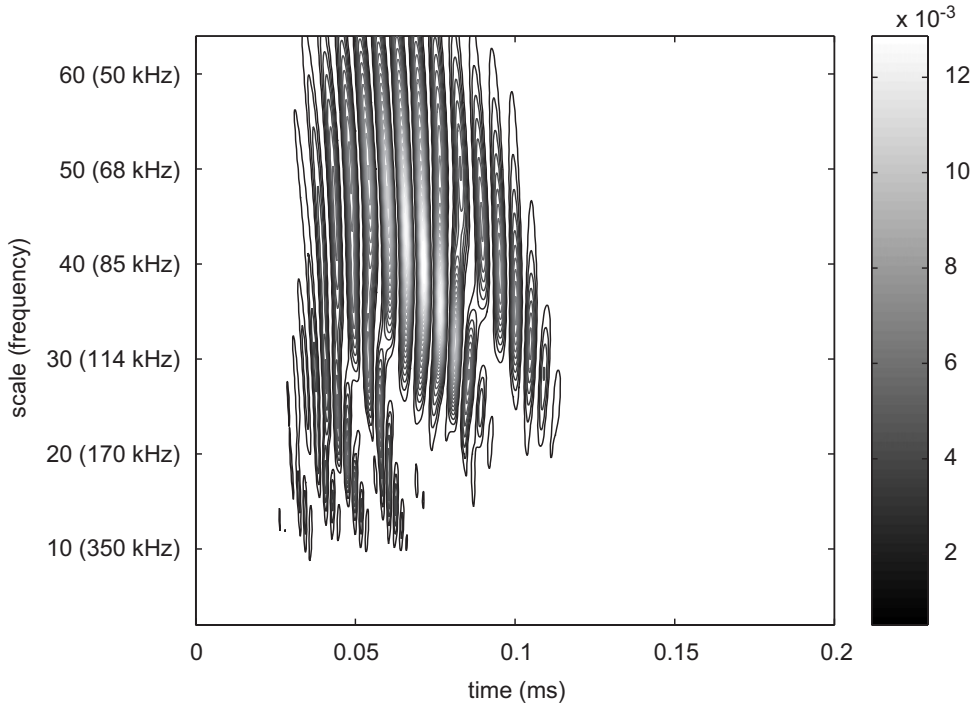


Fig. 15. Time-scale representation provided by the continuous wavelet transform: A signal representative of matrix cracking.

involving the conjugate mirror filters used for the filter bank multiresolution approach [32]. Thus, a CWT is applied to the typical A (matrix cracking) and B (fiber-matrix debonding) AE signals identified above (61 signals) with a scale parameter varying from 2 to 64 by 1 step (Figs. 15 and 16).

The time-scale representations obtained show, at different scales, high energy areas corresponding to the different damage mechanisms. The scales involved are more stretched for the A signals than for the B signals. A signals, representative of matrix cracking, are mainly in the scale range from 25 to 60, referring to the frequency range 50–150 kHz, while B signals, representative of debonding, are in the scale range 10–20, referring to the frequency range 170–350 kHz. A signals exhibit lower frequencies than B signals. These time-scale distributions also show that the most energetic components appear at the beginning of the B waveforms while they appear in the middle for the A signals. The time-scale representation highlights qualitative

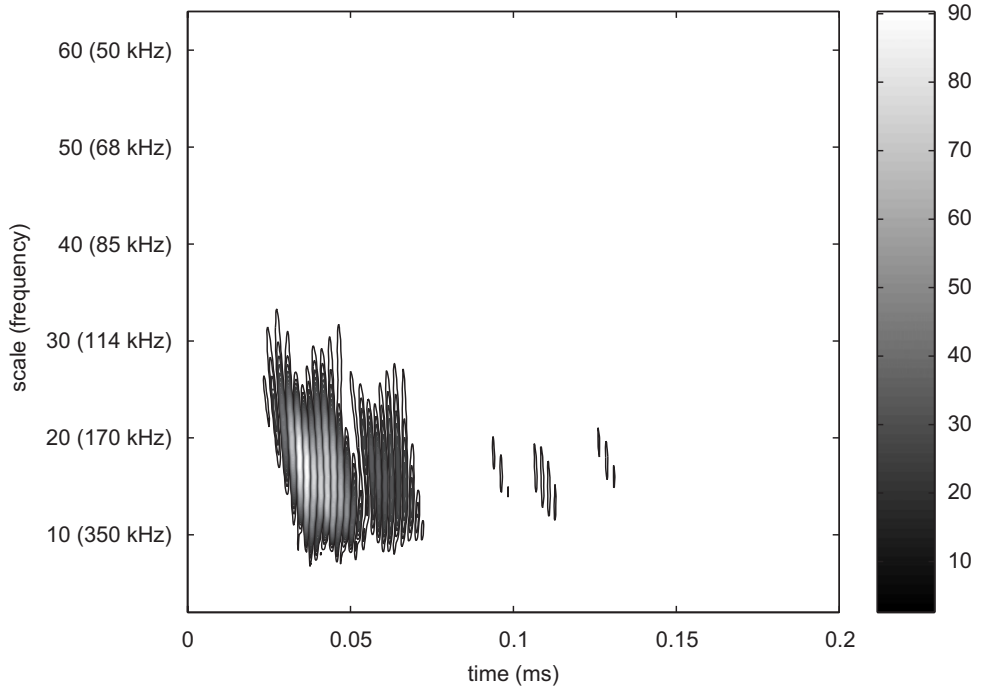


Fig. 16. Time-scale representation provided by the continuous wavelet transform: B signal representative of fiber-matrix debonding.

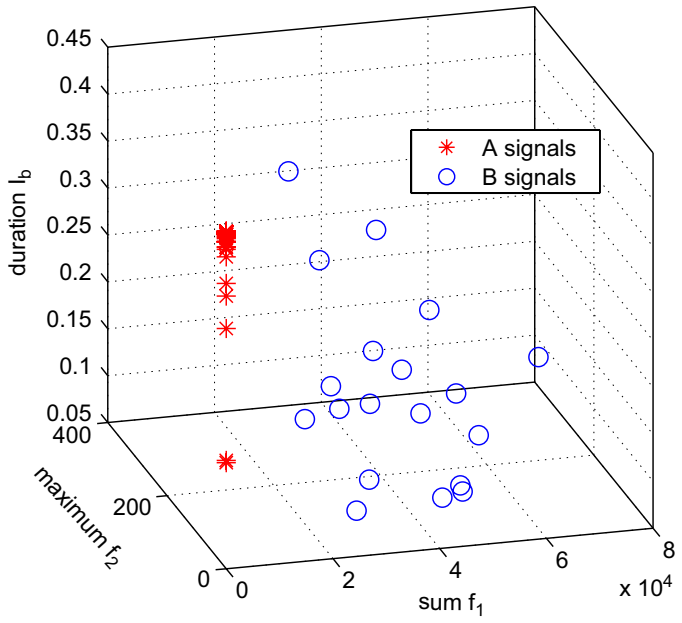


Fig. 17. Visualization of the descriptors: duration $I_b$, sum $f_1$ and maximum $f_2$ of the square moduli of CWT coefficients of a sample of A and B AE signals representative of matrix cracking and fiber-matrix debonding.

differences between the two signatures from matrix cracking and fiber-matrix debonding. To provide an objective measurement of these differences, some time-scale descriptors are extracted from the representation. The first feature is the sum of the square moduli of CWT coefficients defined as follows:

$$f_1(a, I_b) = \sum_b |CW_f(a,b)|^2, \quad b \in I_b. \tag{17}$$

The second feature is the maximum of the square moduli of CWT coefficients

$$f_2(a, I_b) = \max|CW_f(a,b)|^2, \quad b \in I_b. \tag{18}$$

Both are calculated for each scale on a limited time duration $I_b$. This duration is set from an adaptive threshold which corresponds to a percentage (10%) of the maximum amplitude of the wavelet coefficients. Indeed the duration of the AE signal corresponds to the time during which the amplitude of the wavelet coefficients goes beyond the threshold. Then the features corresponding to the most energetic scale are selected as new descriptors. For the previous A (matrix cracking) and B (debonding) signals, two scales are considered: $a = 18$ (190 kHz) for feature $f_1$ and $a = 36$ (95 kHz) for feature $f_2$ (Fig. 17).

The two types of damage mechanisms are well discriminated with these new time-scale descriptors and are better identified than with usual time descriptors.

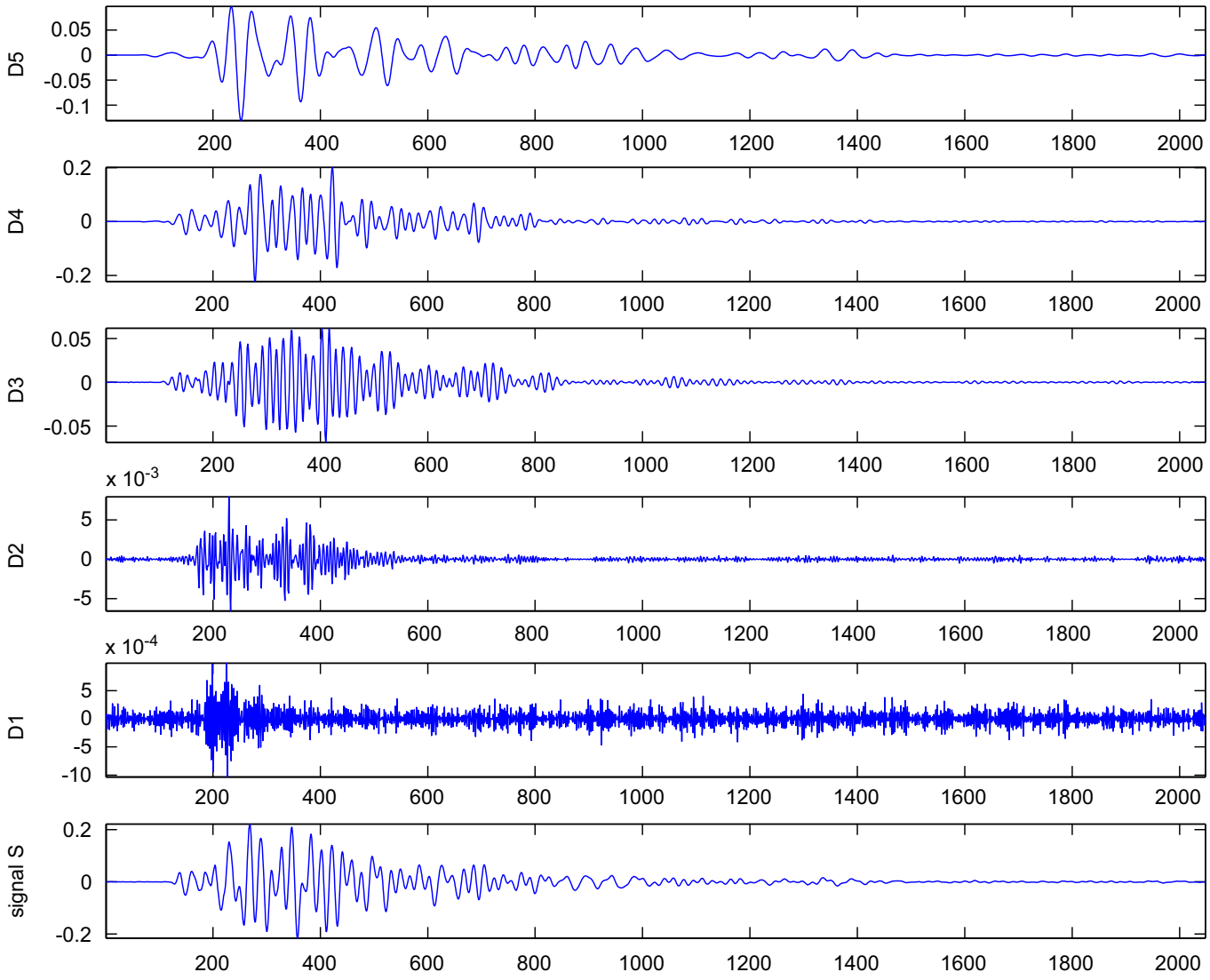


Fig. 18. Five levels wavelet decomposition of a signal (S) (amplitude in V vs. samples): A signal representative of matrix cracking.

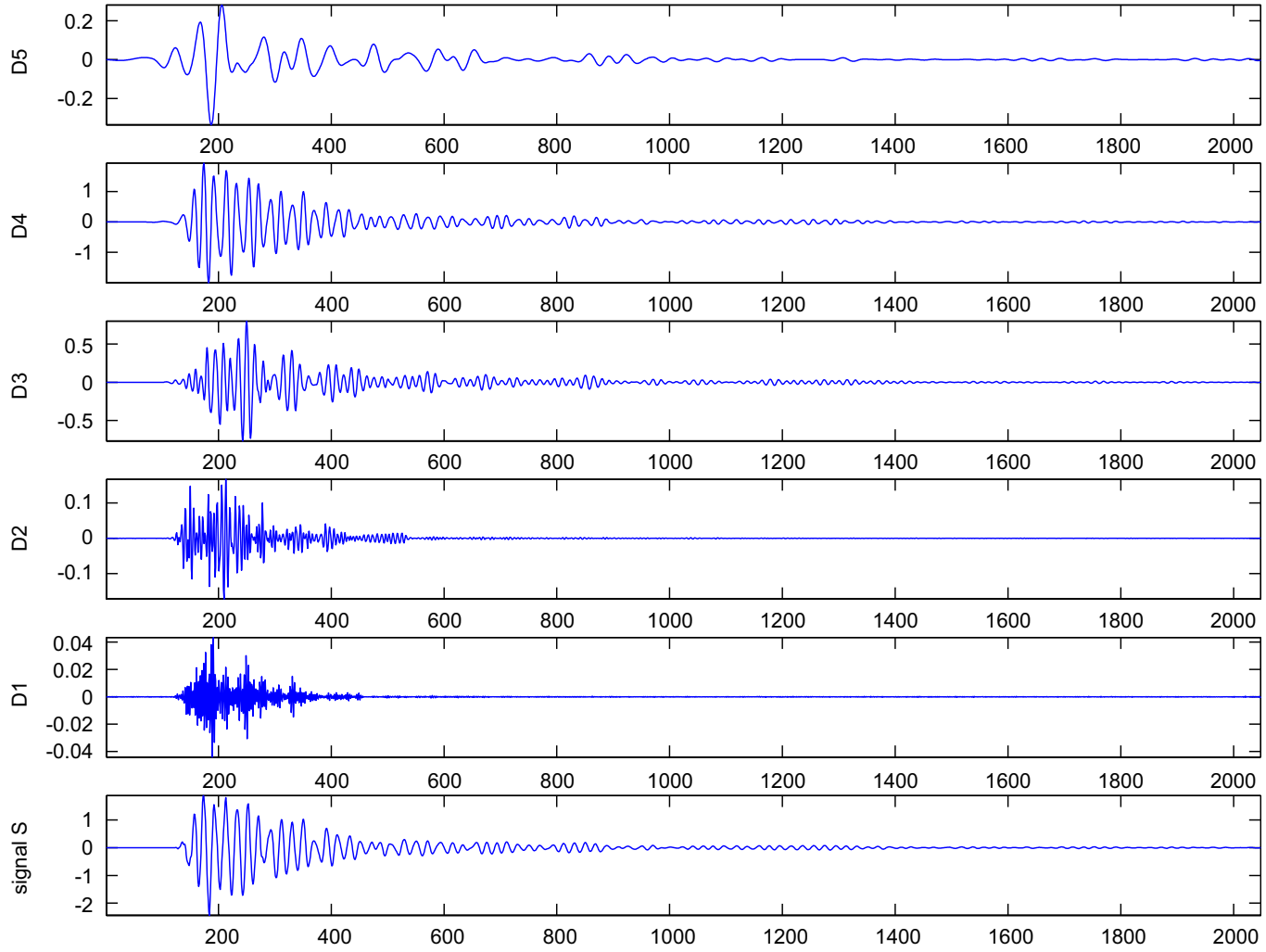


Fig. 19. Five levels wavelet decomposition of a signal (S) (amplitude in V vs. samples): B signal representative of fiber-matrix debonding.

### 4.2.2. Discrete wavelet transform

The use of a DWT enables to decompose each signal on a wavelet basis [32]. The DWT is defined as

$$DW_f(j,k) = \int_{-\infty}^{\infty} f(t)\psi_{j,k}^*(t)\,\mathrm{d}t, \quad \psi_{j,k}(t) = 2^{-j/2}\psi(2^{-j}t - k), \tag{19}$$

where $DW_f(j,k)$ are the coefficients of the wavelet transform, $j$ represents the scale and $k$ the shift in time, $f(t)$ is the analyzed signal and $\psi(t)$ is the analyzing wavelet. The DWT decomposes the analyzed signal into different continuous frequency bands which depend on the level of decomposition. The original signal passes through two complementary filters and two signals are obtained, corresponding to the approximation and the detail coefficients of the first level. At the next resolution, the two filters are applied to the resulting approximation coefficients and so on. The approximations are the high scale, low frequency components of the signal. The details are the low scale, high frequency components. The sum of the signals obtained at each level reconstructs the primary AE signal. The details of the decomposition can be expressed as

$$DTW_f(j,k) = \sum_{n=0}^{N-1} f(n)\psi_{j,k}^*(n), \tag{20}$$

where $DTW_f(j,k)$ is the DWT and $N$ is the number of samples in the signal. The Daubechies wavelets are used for the decomposition. Figs. 18 and 19 show the decomposition of A (matrix cracking) and B (fiber-matrix debonding) AE signals on five levels.

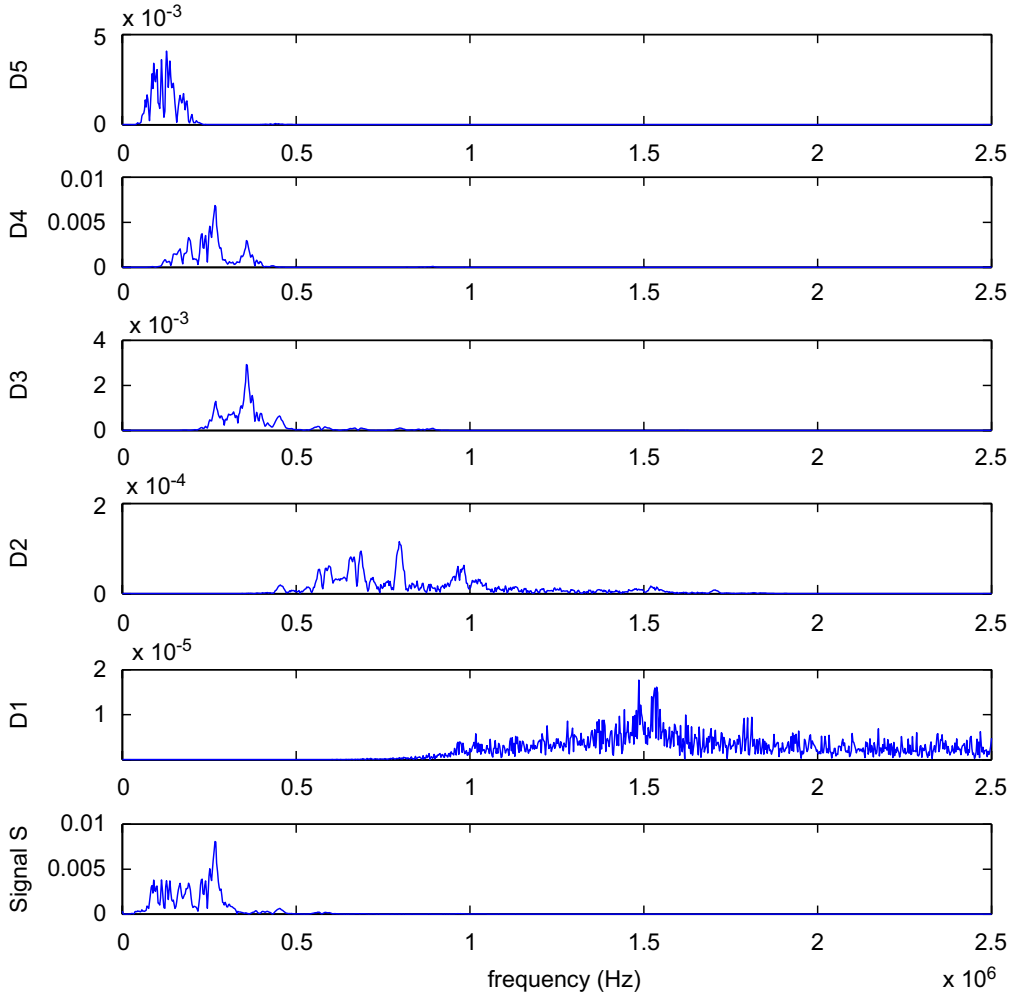


Fig. 20. Modulus of the FFT of the signal (S) and each decomposition level (D1–D5): A signal representative of matrix cracking.

By applying a fast Fourier transform on each detail coefficient, the frequency band associated to each level of decomposition is highlighted. The details D5–D1 have increasing frequency bands up to 2.5 MHz (Figs. 20 and 21).

With this decomposition, the most important frequencies in a signal are highlighted. The B signal, referring to fiber-matrix debonding, has more information into the details D3 and D4 (156–625 kHz). The same study on A signals, referring to matrix cracking, shows a lowest frequency range from 78 to 312 kHz (details D4 and D5). These frequency bands are characteristic of each damage mechanism. The DWT could also provide new relevant descriptors to add in the clustering analysis. Thus, an another feature is defined: the maximum of the square detail coefficients for each level of decomposition. This new descriptor is defined as follows:

$$f_3(j) = \max_k (DTW_f(j,k)^2), \tag{21}$$

where $DTW_f(j,k)$ are the detail coefficients of each level of decomposition $j$. Indeed, we have shown that the square detail coefficients have their maximum value in different frequency bands for each kind of signal. Thus, this was the clue to find this relevant parameter $f_3$, in which the maximum value of the square detail coefficients is calculated for the levels of decomposition with the most significant amplitude (D3–D5).

### 4.3. Clustering of AE data

In this part, we establish a comparison between the PCA results for clustering represented in two feature spaces: one from the time-scale descriptors, the other one from the traditional temporal AE features.

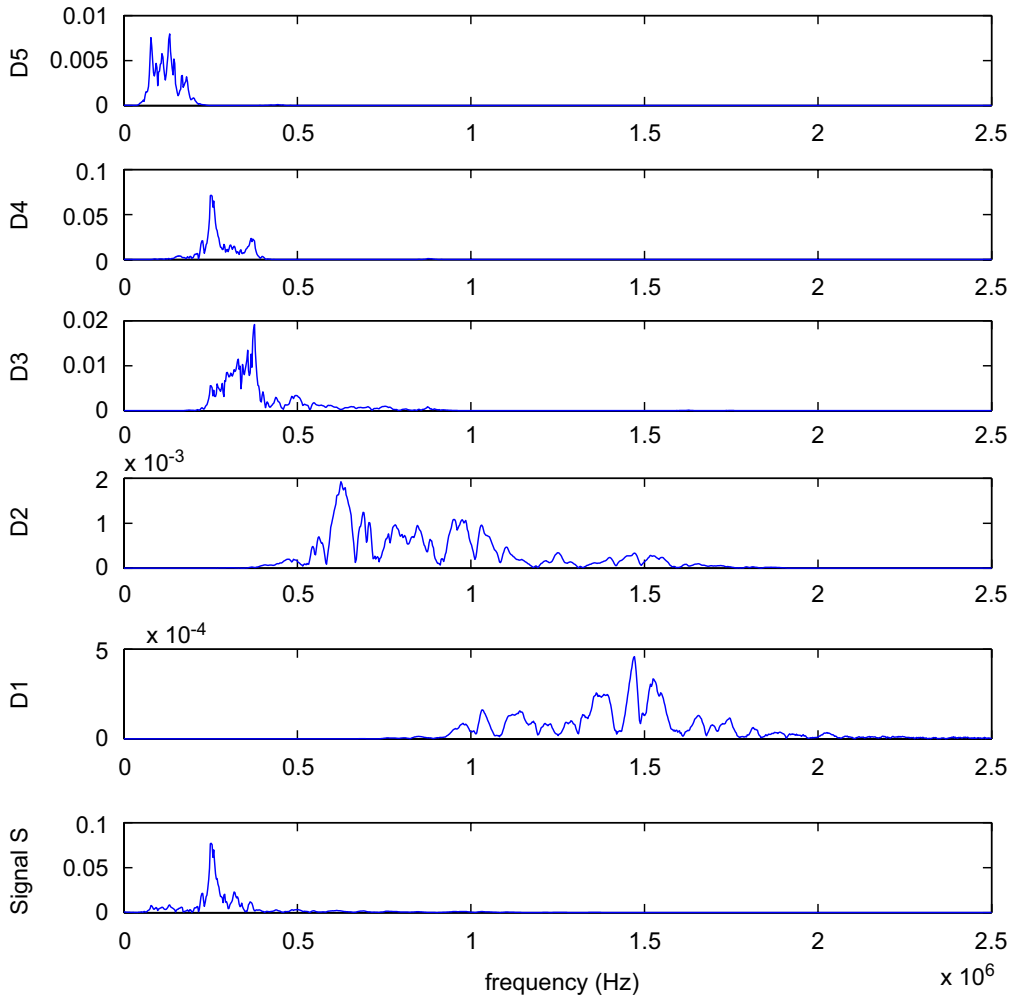


Fig. 21. Modulus of the FFT of the signal (S) and each decomposition level (D1–D5): B signal representative of fiber-matrix debonding.

The analysis is first applied to a sample of known AE signals and then to random AE events collected from a static three-point bending test on an actual material as the cross-ply composite material.

*4.3.1. Clustering of a sample of known AE signals*

A PCA is used to visualize the patterns composed of six new time-scale features: duration $I_b$, sum and maximum of the square moduli of CWT coefficients (feature $f_1$ and $f_2$) and maximum of the square DWT detail coefficients (feature $f_3$ for the three levels D3–D5) for a sample of 60 A (matrix cracking) and B (fiber-matrix debonding) AE signals. The result is shown in the top of Fig. 22, where A and B known signals are represented by different plot symbols. This PCA projection shows that the distribution of the data does not overlap. Thus, classifying the data and separating the damage mechanism seems easier as it is shown in the bottom of Fig. 22, which represents the PCA visualization of the fuzzy C-means clustering on the sample of AE signals.

To establish a comparison, this study is also made with the traditional temporal AE descriptors from the same sample of 60 AE signals. The result is presented in Fig. 23. The top figure illustrates the PCA projection of the patterns composed of temporal descriptors: the amplitude, the rise time, the counts and the duration of the signals. The bottom figure highlights the fuzzy C-means clustering in the same representation space. These figures show that the separation between the two classes is less obvious and that some patterns are assigned to the wrong cluster. This is probably due to the fact that the calculation of the temporal descriptors is very dependent on the amplitude threshold used to detect the arrival time and the end of an AE signal by the data

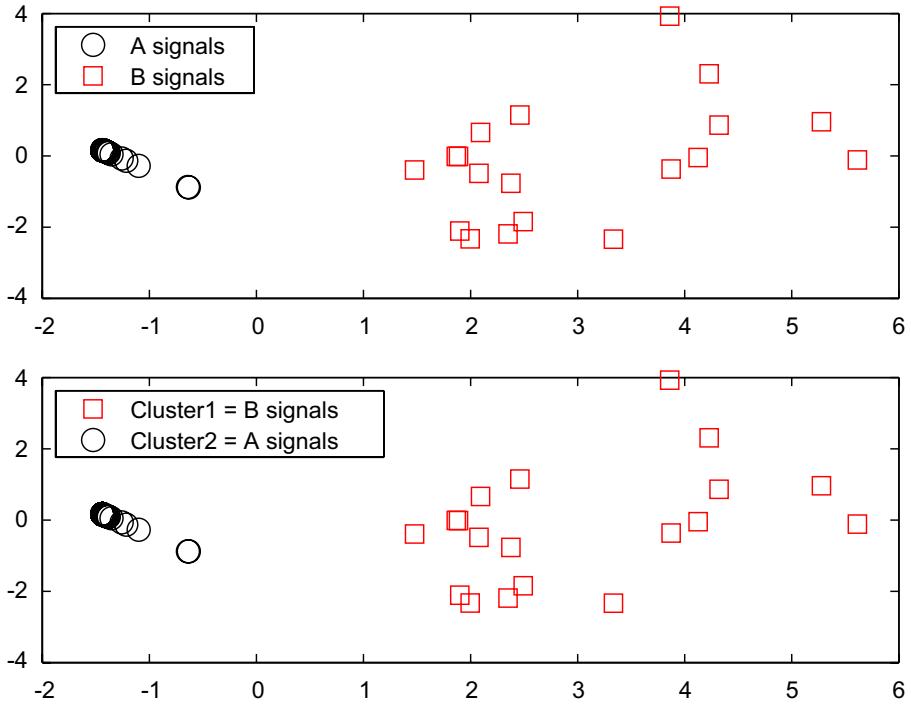


Fig. 22. Top: PCA visualization of new time-scale descriptors (93% information kept) of a sample of A and B AE signals representative of matrix cracking and fiber-matrix debonding. Bottom: PCA visualization of the fuzzy C-means clustering.

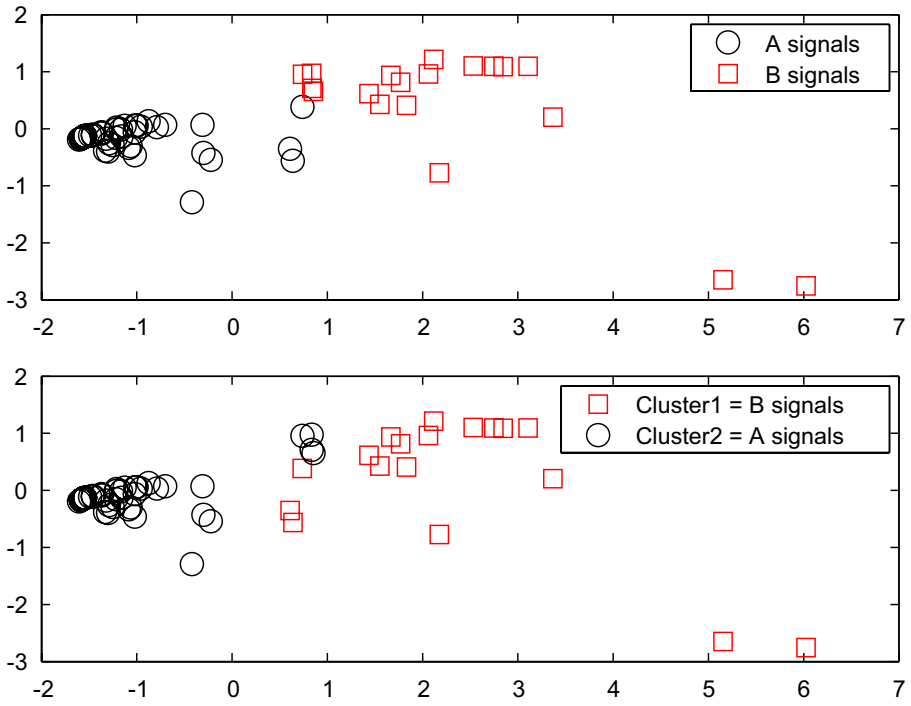


Fig. 23. Top: PCA visualization of temporal descriptors (94% information kept) of a sample of A and B AE signals representative of matrix cracking and fiber-matrix debonding. Bottom: PCA visualization of the fuzzy C-means clustering.

acquisition system. Except the patterns located in the area between the two classes in the time-based feature space, each pattern of the data set is assigned to the same cluster (matrix cracking or fiber-matrix debonding) whatever feature space is used.

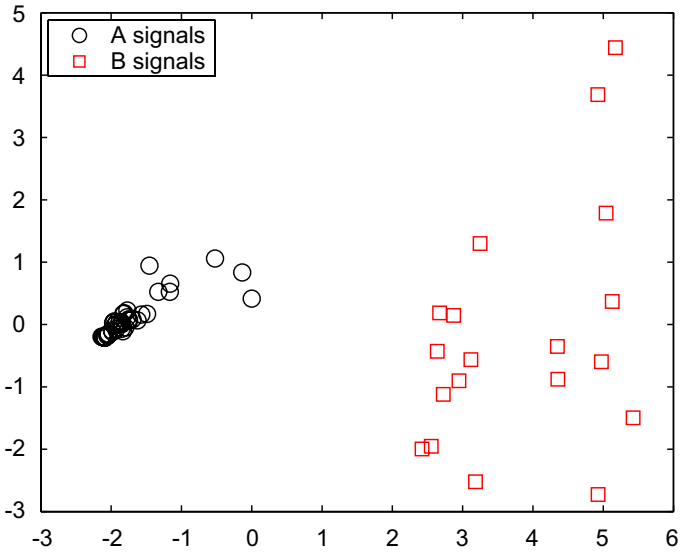


Fig. 24. PCA visualization of the fuzzy C-means clustering with both temporal and time-scale descriptors of a sample of A and B AE signals representative of matrix cracking and fiber-matrix debonding (93% information kept).

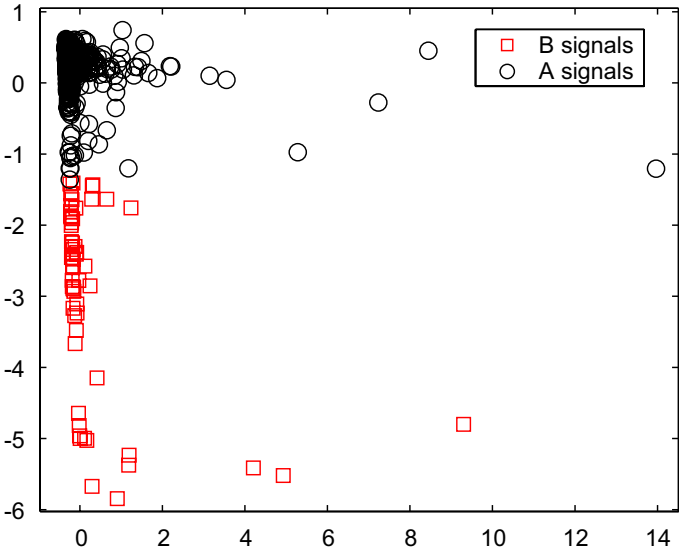


Fig. 25. PCA visualization of the fuzzy C-means clustering with time-scale descriptors on 729 AE events (94% information kept). A signal is representative of matrix cracking and B signal of fiber-matrix debonding.

Finally, the fuzzy C-means clustering is applied with both the time-scale and the traditional temporal descriptors on the sample of AE signals. The PCA projection is shown in Fig. 24. The result is very similar to the one obtained with only the time-scale descriptors.

*4.3.2. Clustering of cross-ply composite material*

In what follows, the FCM is applied with two clusters that correspond to the two damage mechanisms: matrix cracking (A signals) and fiber-matrix debonding (B signals) on 729 AE events from a static three-point bending test on a cross-ply composite material. One must note that in this experiment because of the low thickness of the samples no delamination was generated. The time-scale descriptors presented above ($f_1, f_2, f_3$ and $I_b$) are used for the classification. A PCA is achieved in order to visualize the results in a two-dimension subspace (Fig. 25). The time dependency of the two damage types is also shown in the material (Fig. 26). The two damage mechanisms are well identified in the material. Indeed, the PCA projection highlights the

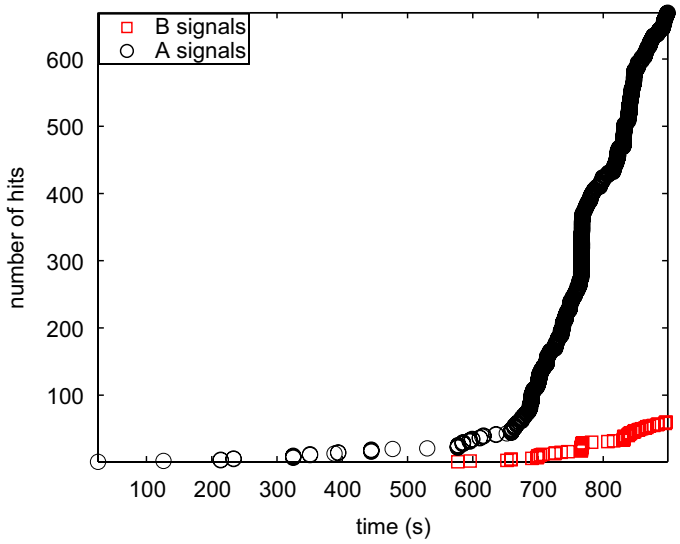


Fig. 26. Time dependency of the identified damage types with time-scale descriptors on 729 AE events. A signal is representative of matrix cracking and B signal of fiber-matrix debonding.

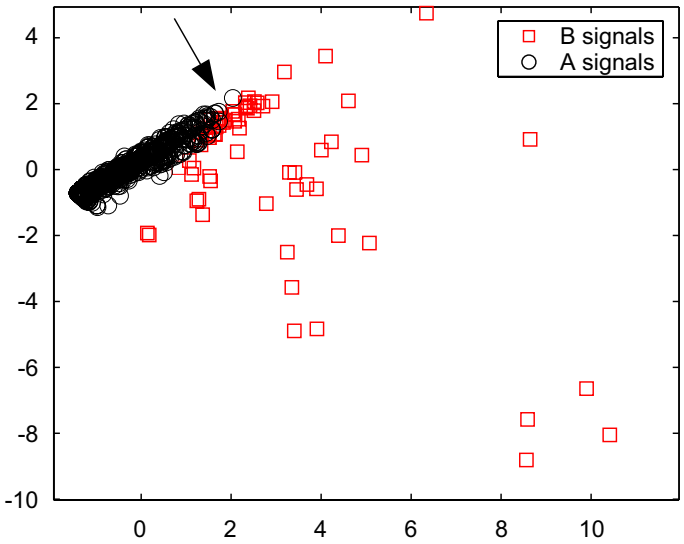


Fig. 27. PCA visualization of the fuzzy C-means clustering with temporal descriptors on 729 AE events (90% information kept). A signal is representative of matrix cracking and B signal of fiber-matrix debonding.

similarities between the patterns. In addition, there is no overlap between the data with these time-scale descriptors.

The PCA results for clustering on the same AE data set with the traditional temporal AE features are also given in Fig. 27. The five descriptors used are the energy, the amplitude, the rise time, the counts and the duration of the signals. The time dependency of the two damage types is not shown but it is similar to Fig. 26. In comparison with the clustering made with the use of time-scale descriptors, the PCA projection shows that some patterns are mixed with each other (see the area near the black arrow in Fig. 27). Thus, with the temporal descriptors, the separation between the patterns is not effective in this area. The two classifications provided by clustering are different: 2.5% less patterns are classified as B signals (debonding) with the use of temporal descriptors.

## 5. Conclusion

FCM is coupled with a PCA to discriminate different damage mechanisms from AE signals and to visualize the classification into classes. Clustering is first done with the typical temporal descriptors of AE waveforms.

The resulting clusters clearly identify the damage mechanisms in complex composite materials: SMC and cross-ply composites under creep tensile tests. This unsupervised method also shows the time evolution of damage mechanisms in these materials till the global failure. Thus the most critical damage mechanisms are identified. However, AE signals in composite materials are not stationary. The temporal descriptors used are not always relevant. Thus, wavelet analysis of AE signals is applied in order to improve the discrimination of damage mechanisms. The CWT and DWT are applied on typical matrix cracking and fiber-matrix debonding AE signals. These two kinds of signals are clearly identified and show different frequency bands. New time-scale descriptors are defined and extracted from each time-scale representation of AE signals. The time-scale descriptors are more relevant and discriminate very well the alike damage mechanisms which are more difficult to separate with the usual temporal descriptors. The perspectives of this work are to define more relevant time-frequency or time-scale descriptors to include them in the clustering method in order to improve the identification of damage mechanisms of actual composite materials and other structural materials as concretes.

## Acknowledgements

We gratefully acknowledge R. Berbaoui and M. Assarar from the Groupe Composites et Structures Mécaniques de l'Université du Maine (France), for the elaboration of the glass/polyester composite samples and for their involvement in the mechanical and acoustic emission experiments.

## References

[1] K. Ono, Acoustic emission, Encyclopedia of Acoustics, Wiley, New York, 1997.
[2] A.G. Beattie, Acoustic emission, principles and instrumentation, Journal of Acoustic Emission (1/2) (1983) 95–128.
[3] N. Ativitavas, T. Fowler, T. Pothisiri, Acoustic emission characteristics of pultruded fiber reinforced plastics under uniaxial tensile stress, in: Proceedings of European WG on AE, Berlin, 2004, pp. 447–454.
[4] D.-J. Yoon, W. Weiss, S.P. Shah, Assessing damage corroded reinforced concrete using in acoustic emission, Journal of Engineering Mechanics (2000) 273–283.
[5] A.G. Magalhaes, M.F. de Moura, Application of acoustic emission to study creep behaviour of composite bonded lap shear joints, NDT&E International 38 (2005) 45–52.
[6] A. Calabro, C. Esposito, A. Lizza, M. Giordano, A. D'Amore, L. Nicolais, Analysis of the acoustic emission signals associated to failure modes in CFRP laminates, in: ECCM, vol. 8, 1997, pp. 425–432.
[7] S. Barre, M.-L. Benzeggagh, On the use of acoustic emission to investigate damage mechanisms in glass-fiber reinforced polypropylene, Composites Science and Technology 52 (1994) 369–376.
[8] H. Nechad, A. Helmstetter, R. El Guerjouma, D. Sornette, Creep ruptures in heterogeneous materials, Physical Review Letters 94 (2005).
[9] R. El Guerjouma, J.C. Baboux, D. Ducret, N. Godin, P. Guy, S. Huguet, Y. Jayet, T. Monnier, Non-destructive evaluation of damage and failure of fiber reinforced polymer composites using ultrasonic waves and acoustic emission, Advanced Engineering Materials 3 (2001) 601–608.
[10] N. Godin, S. Huguet, R. Gaertner, L. Salmon, Clustering of acoustic emission signals collected during tensile tests on unidirectionnal glass/polyester composites using supervised and unsupervised classifiers, NDT&E International 37 (2004) 253–264.
[11] V. Kostopoulos, T.H. Loutas, A. Kontsos, G. Sotiriadis, Y.Z. Pappas, On the identification of the failure mechanisms in oxide/oxide composites using acoustic emission, NDT&E International 36 (2003) 571–580.
[12] M. Johnson, Waveform based clustering and classification of Ae transients in composite laminates using principal component analysis, NDT&E International 35 (2002) 367–376.
[13] K. Ono, Q. Huang, Pattern recognition analysis of acoustic emission signals, in: Progress in Acoustic Emission VII, The Japanese Society for NDI, 1994, pp. 69–78.
[14] Y.Z. Pappas, Y.P. Markopoulos, V. Kostopoulos, Failure mechanisms analysis of 2D carbon/carbon using acoustic emission monitoring, NDT&E International 31 (1998) 157–163.
[15] N. Godin, S. Huguet, R. Gaertner, Integration of the Kohonen's self-organising map and k-means algorithm for the segmentation of the AE data collected during tensile tests on cross-ply composites, NDT&E International 38 (2005) 299–309.
[16] T. Kohonen, Self-organized network, in: Proceedings of the IEEE, vol. 43, 1990, pp. 59–69.
[17] A. Likas, N. Vlassis, J. Verbeek, The global k-means clustering algorithm, Pattern Recognition 366 (2) (2003) 451–461.
[18] B. Dubuisson, Diagnostic, intelligence artificielle et reconnaissance des formes, Hermès Science Publications, 2001.
[19] J.C. Bezdek, Pattern Recognition with Fuzzy Objective Function Algorithms, Plenum Press, New York, 1981.
[20] I.T. Jolliffe, Principal Component Analysis, Springer, Berlin, 1986.
[21] E. Oja, Neural networks, principal components, and subspaces, International Journal of Neural Systems 1 (1989) 61–68.

[22] C. Ramirez-Jimenez, N. Papadakis, N. Reynolds, Identification of failure modes in glass/polypropylene composites by means of the primary frequency content of the acoustic emission events, Composites Science and Technology 64 (2004) 1819–1827.
[23] J. Bohse, Damage analysis of polymer matrix composites by acoustic emission testing, in: Proceedings of European WG on AE, Berlin, 2004, pp. 339–348.
[24] M. Giordano, A. Calabro, C. Esposito, A. D'Amore, L. Nicolais, An acoustic-emission characterization of the failure modes in polymer-composite materials, Composites Science and Technology 58 (1998) 1923–1928.
[25] Q.-Q. Ni, M. Iwamoto, Wavelet transform of acoustic emission signals in failure of model composites, Engineering Fracture Mechanics 69 (2002) 717–728.
[26] P.J. De Groot, P.A.M. Wijnen, R.B.F. Janssen, Real time frequency determination of acoustic emission for different fracture mechanisms in carbon/epoxy composites, Composites Science and Technology 55 (1995) 405–412.
[27] M.A. Hamstad, A. O'Gallagher, J. Gary, A wavelet transform applied to acoustic emission signals: part 1: source identification, Journal of Acoustic Emission 20 (2002) 39–61.
[28] D.B.B. Ferreira, R.R. Da Silva, J.M.A. Rebello, M.H.S. Siqueira, Failure mechanism characterisation in composite materials using spectral analysis and the wavelet transform of acoustic emission signals, INSIGHT 46 (5) (2004) 282–289.
[29] A. Gallego, J.F. Gil, J.M. Vico, J.E. Ruzzante, R. Piotrkowski, Coating adherence in galvanized steel assessed by acoustic emission wavelet analysis, Scripta Materialia 52 (2005) 1069–1074.
[30] H. Suzuki, T. Kinjo, Y. Hayashi, M. Takemoto, K. Ono, Wavelet transform of acoustic emission signals, Journal of Acoustic Emission 14 (1996) 69–84.
[31] R. De Oliveira, C.A. Ramos, A.T. Marques, Applications of the wavelet transform to the modal analysis of clustered AE waveforms, Smart Structures and Systems, 2006, submitted for publication (private communication).
[32] S. Mallat, A Wavelet Tour of Signal Processing, Academic Press, New York, 1998.
[33] T.H. Loutas, V. Kostopoulos, C. Ramirez-Jimenez, M. Pharaoh, Damage evolution in center-holed glass/polyester composites under quasi-static loading using time/frequency analysis of acoustic emission monitored waveforms, Composites Science and Technology 66 (2006) 1366–1375.
[34] G. Qi, A. Barhorst, J. Hashemi, G. Kamala, Discrete wavelet decomposition of acoustic emission signals from carbon-fiber-reinforced composites, Composites Science and Technology 57 (1997) 389–403.
[35] R. Piotrkowski, A. Gallego, E. Castro, M.T. Garcia-hernandez, J.E. Ruzzante, Ti and Cr nitride coating/steel adherence assessed by acoustic emission wavelet analysis, NDT&E International 38 (2005) 260–267.
[36] D. Ducret, R. El Guerjouma, Y. Jayet, J.C. Baboux, Anisotropic damage evaluation in polymer fiber composites under hygrothermal aging by means of ultrasonic techniques, Review of Progress in Quantitative Nondestructive Evaluation 20B (2000) 1199–1206.
[37] A. Nielsen, Acoustic Emission Source based on Pencil Lead Breaking, The Danish Welding Institute Publication, vol. 80, 1980, p. 15.
[38] A.M. Bensaid, L.O. Hall, J.C. Bezdek, L.P. Clarke, M.L. Silbiger, J.A. Arrington, R.F. Murtagh, Validity-guided reclustering with applications to image segmentation, in: Proceedings of the IEEE Transactions on Fuzzy Systems, vol. 4, 1996, pp. 112–123.
[39] M. Suzuki, H. Nakanishi, M. Iwamoto, E. Jinen, Application of static fracture mechanisms to fatigue fracture behavior of class A-SMC composite, in: Proceedings of the 4th Japan–US Conference on Composite Materials, 1988, pp. 297–306.
[40] A. Marec, J.-H. Thomas, R. El Guerjouma, Etude multivariable par émission acoustique de l'endommagement et de la rupture des matériaux composites sollicités en fluage, in: Proceedings of the CFA, 2006, pp. 793–796.
[41] I. Daubechies, Ten Lectures on Wavelets, SIAM, Philadelphia, PA, 1992.